Electrospinning of polymeric nanofiber (nylon 6,6/graphene oxide) for removal of Cr (VI): synthesis and adsorption studies

Şerife Parlayıcı[1], Ahmet Avcı[2] and Erol Pehlivan[1*]

Abstract

Polymer nanofibers are valuable materials that are of great importance because they are inexpensive and they display high strength. In this study, nylon-6,6 (N6,6)/graphene oxide (GO) nanofibers were developed and characterized. GO was synthesized from graphene using the known Hummer's method. GO is obtained by reaction of the graphene with strong oxidants and was characterized using Fourier-transform infrared spectroscopy (FT-IR) and scanning electron microscopy (SEM). The characterizations showed that the graphene was suitably oxidized. GO was added to N6,6 to produce N6,6/GO nanofibers at loadings of 0.5, 1.0, 1.5, and 2.0 wt% through the melt mixing method. The batch adsorption model for Cr (VI) adsorption was applied as a function of time, initial Cr (VI) concentration, adsorbent dosage, and pH to examine nanofiber activity. N6,6/GO a exhibited high adsorption capacity for Cr (VI) at pH 2.0. The maximum adsorption capacity for Cr (VI) ion was found to be 47.17 mg/g of N6.6/GO using the related isotherm curves and equations. When the equilibrium data were examined, it was concluded that Langmuir adsorption isotherm was more suitable.

Keywords: Graphene oxide, Nanocomposite, Adsorption, Chromium, Nylon 6,6

Introduction

There is a grade demand to use corrosion-resistant and solvent-resistant low-density organic materials for simple installation and industrial purposes. Recently, graphene-doped materials have been broadly used in semiconductors and nanofibers (Coiai et al. 2015). Semi-crystalline polymers contain a huge number of organic materials including crystalline and amorphous molecular structures. Polyolefin, polyester, polyamide, and vinyl are some examples of imperative groups of organic semi-crystalline polymers. It is well-known that semi-crystalline polymers are liable for the crystal phase charge transfer, that is, mechanical and non-viscous mechanical behaviors capable of applying incredible physical force depends on this phase response (Pouriayevali et al. 2013). For this reason, it is important to enter into details about the crystal phase of semi-crystalline materials used in industry. Recently, polyamides (nylon) as a group of semi-crystalline polymers joined with nanomaterials have received great

interest due to their extensive applications. Nanocomposite polymers have high mechanical properties such as modulus, strength, and hardness.

In recent years, industrial wastewater harmful components have increased particularly in developing countries. For this reason, desalination of the water is one of the foremost promising chemical actions to provide clean water for dry areas. Various desalting strategies for removing dissolved solids, like reverse osmosis (Pontiéa et al. 2013) and pressure differences (Syrwade et al. 2015), membrane separation (Korus and Loska 2009), electrodialysis (Nataraj et al. 2007), reverse osmosis (Hafez and El-Manharawy 2004), chemical precipitation (Vasudevan et al. 2012), and ion exchange (Oehmen et al. 2014) are well known strategies applied for wastewater purification or remediation. The new two-dimensional graphite plates were applied as a chemically modifiable desalination material because of their extremely strong and unique physical and mechanical properties (Konatham et al. 2013). However, current strategies have disadvantages like a high operative and capital cost, restricted tolerance to the hydrogen ion concentration range of wastewater,

* Correspondence: erolpehlivan@gmail.com
[1]Department of Chemical Engineering, Konya Technical University, 42079 Konya, Turkey
Full list of author information is available at the end of the article

incomplete metal removal percentage, and a huge quantity of energy demand. Hence, the adsorption techniques using modified organics are currently about to be a good, efficient, and economic methodology for harmful metal treatment method (Luo and Lü 2015). N6,6/GO offers flexibility in style, ease of use, and leading to high-quality refined wastewater. Adsorbent materials containing activated carbon (Huang et al. 2007; Gerçel et al. 2007), zeolites (Panuccio et al. 2009), chitosan (Bamgbose et al. 2010), and lignocellulose (Shin et al. 2007) were tested and developed within a previous couple of decades. However, most of those adsorbents do not seem to be effective in water purification systems and there is no effective diffusion or limitation of effective surface areas. They have caused issues like difficulty in remediation from effluents or the production of secondary wastes.

GO is obtained by treating graphite with sturdy oxidizers. the word "oxide" is inaccurate used word however traditionally established in science because graphite is not a metal. The bulk material disperses in basic solvent yielding GO. Starting from the graphite, ultrasonic agitation is the most suitable option for GO production. GO is a compound composed of organic atoms like C, O, and H at numerous ratios, typically is obtained by process graphite with sturdy oxidizers. The bulk volume of them disperses in basic medium yielding monomolecular sheets, called as GO by similarly to graphene, the single-layer form of graphite (Ma et al. 2013). GO layers have shown an increasing interest as a possible intermediate for the production of graphene in the near future (Chen et al. 2018). The termination of every layer has carboxyl and carbonyl groups. N6,6 has an excellent mechanical resistance because of hydrogen bonds and their cross-linking and the long chains being brought along for attraction (Menchaca et al. 2006).

Electrospinning is a noted technique to produce polymer fibers ranging in diameter from 40 to 2000 nm. Electrospinning starts once the electric force of the mother liquid surface exceeds the surface tension and initiates an electric spark provoking the solution to be expelled from the syringe, and a jet flows and therefore the nanofibre is collected on a metal screen. To take advantage of the properties of each material, N6,6 and GO were combined as a hybrid nanocomposite (Nirmala et al. 2015).

In this work, the selective N6,6/GO nanocomposite has been applied with success in the removal method and Cr (VI) adsorption from the aqueous solution with pH, time, and adsorbent quantity have been investigated. There are no reports on the work of N6,6/GO interaction for the Cr (VI) adsorption. N6-6 has a high mechanical resistance due to the mutual attraction of its long chains. By combining the properties of N6,6/GO, a new hybrid material was produced. This nanocomposite has some functional groups such as such as a carboxyl group (-COOH), a hydroxyl group (-OH), an amine group (-NH), and a carbonyl group (-CO) which may interact with Cr (VI) ion.

Materials and methods
Materials
N6,6 from Sigma-Aldrich and DMF from Sigma-Aldrich were purchased and all other chemicals (NaOH, HCl, formic acid, chloroform) were purchased from Merck Company. We produced GO in our laboratory. Figure 1 shows the structure of N6,6, graphene, and GO. Ultrapure water was used for preparation of Cr (VI) stock solution and other solutions. The stock Cr (VI) solution was originated by dissolving $K_2Cr_2O_7$ salt (purity: $\geq 99.9\%$) (Merck) in pure water. For pH adjustment of solution phase, 0.1 M NaOH and HCl solutions were added in the prepared Cr (VI) solutions.

N6,6/GO electrospun nanocomposite production
Glassman High Voltage Inc. brand power supply unit and AC/DC current power supply (in Fig. 2) were used to obtain 1–50 kV and 0.1–100 mA. Universal 801 syringe pump was used to receive a fixed quantity of
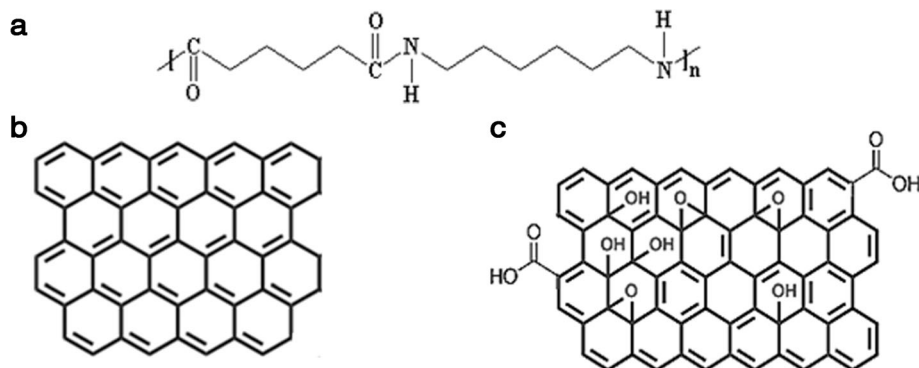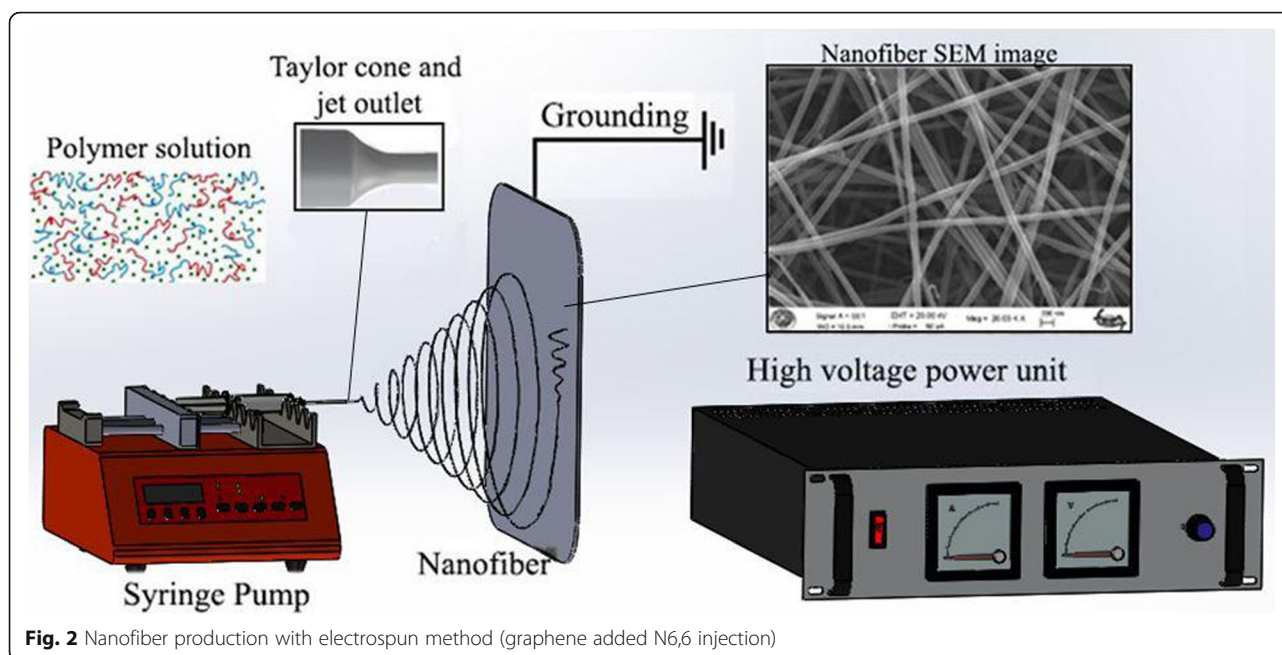

Fig. 1 Chemical structures. a N6,6. b Graphene. c GO

Fig. 2 Nanofiber production with electrospun method (graphene added N6,6 injection)

solution from the syringe tip. Electrospinning polymer is a technique for long and continuous nanofiber production. The high voltage power supply consists of two main sections; electrospinning and a syringe pump. After preparing the polymer solution in a suitable container, it was placed inside a syringe or capillary tubing and then connected to a high voltage power supply. An electrical field was created between the grounded collector (anode) and the tip of the syringe (negative pole). The high voltage power supply is critical to provide the force of electrospinning and continuity of spinning. A syringe pump (feeders) is employed to send the polymer solution in the syringe at a selected flow rate of the polymer.
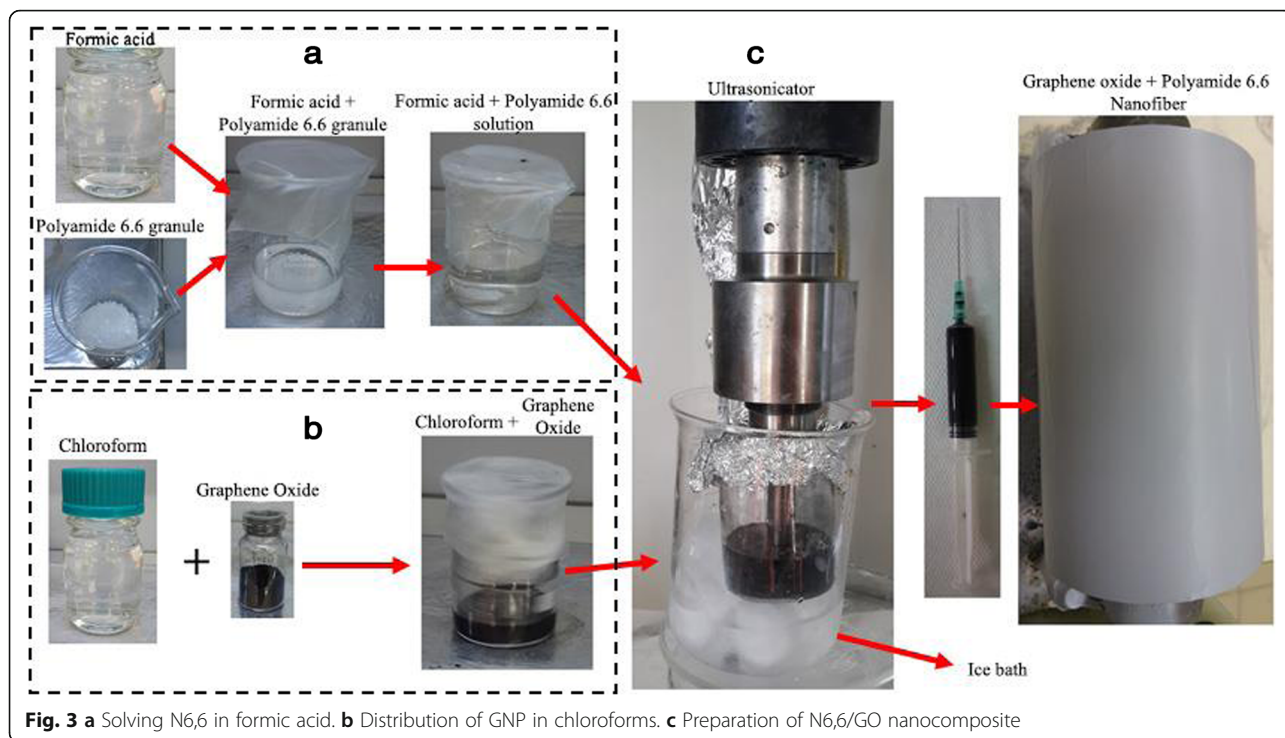
Polymer drops at feeder unit hanging at the tip of the syringe were in a spherical form up to a critical voltage, due to the surface tension force applied. The applied potential difference (high electric field) reaches a threshold worth and also the surface electrostatic forces are synchronic to tension forces. Polymer drops changes to cone shapes at this time. This cone is named Taylor cone. A jet shoots through the tip of Taylor cone and follows totally different paths once it moves between the syringe needle and the collector. On the way, the solvent in the polymer solution evaporates in the air. As the polymer jets get closer to the collector, new polymer jets in nano-diameter forms and they were collected on the grounded conductive collector (Shin et al. 2001).

In this study, the solution preparation method has been started initially by solving of N6,6. As seen in Fig. 3, N6,6 solution was prepared by adding formic acid to 3 g pellets form of N6,6 and the solution was stirred continuously by a magnetic stirrer till they were mixed fully.

At that point, the graphene nanoparticles (GNP) (5 wt%) have been included into 30 mL of formic acid mixed with 9 mL chloroform (Fig. 3a). We added chloroform to the formic acid solution to homogenize the solution before adding N6,6 (Fig. 3b). In that way, the particles can distribute homogeneously throughout the solution. After 10 min of mixing this solution with an ultrasonic blender, N6,6 was added and to the solution then the solution was mixed with a probe appended sonicator (50 kHz frequency) for 1 h. Heat is evolved because of working of the sonicator with sound waves. This heat causes the temperature of the solution to increase. As shown in Fig. 3c, an ice bath was placed at the bottom of the solution vessel to balance the temperature. This prepared solution was taken in 5 mL syringe to obtain nanofiber. In the experimental set-up, a supply pump was adjusted to 1 mL/s speed and the syringe tip is set to be a 12 cm distance from the drum. The high voltage power supply can set to a voltage value of 22 kV to start the nanofiber production. The nanofiber production was carried out at 25 °C in the laboratory.
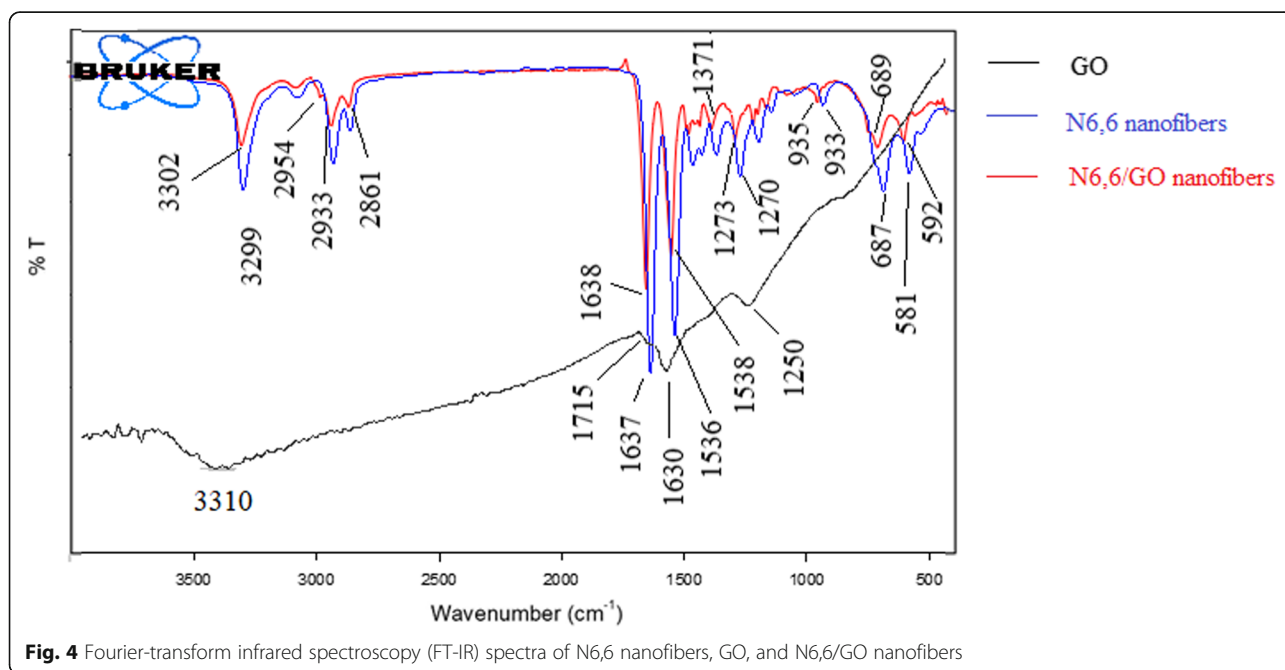
FT-IR studies
The FT-IR is an important analysis for the evaluation of functional groups. The FT-IR spectra of the material were recorded and given in Fig. 4. FT-IR proves the chemical structure of GO showing the metal binding chemical groups such as O-H bonds at 3310 cm^{-1}, the stretching vibrations of -COOH bonds at 1715 cm^{-1}, stretching vibration of C=C bonds at 1630 cm^{-1} (Liu et al. 2018), and -C-O stretching vibration at 1250 cm^{-1} (He et al. 2015). FT-IR

Fig. 3 a Solving N6,6 in formic acid. **b** Distribution of GNP in chloroforms. **c** Preparation of N6,6/GO nanocomposite

indicated the chemical structure of the nylon 6,6, with the certain chemical groups such as N–H stretching peaks at 3299 cm^{-1}, C–H stretching at 2861–2933 cm^{-1}, amide-I at 1637 cm^{-1}, amide-II at 1536 cm^{-1} (Haggenmueller et al. 2006), and amide-III at 1370 cm^{-1}, O=C–H at 581 cm^{-1}, C–C at 687 cm^{-1} (Charles et al. 2009). FT-IR confirmed the chemical groups related to the N6,6/GO nanocomposite such

as the bands at 1638 cm^{-1} are assigned to C=C skeletal stretching. The broad peak at 2954 cm^{-1} shows the stretching vibrations of -OH bonds. The peaks at 1371 cm^{-1} reflect the carboxylic acid groups due to the O–H in-plane deformation and C=O stretching vibration (Shin et al. 2001; Chen et al. 2010). The O=C–H broad peak and C–C stretching peaks appeared at 592 cm^{-1} and 689 cm^{-1}, respectively.

Fig. 4 Fourier-transform infrared spectroscopy (FT-IR) spectra of N6,6 nanofibers, GO, and N6,6/GO nanofibers

SEM-EDX analysis

SEM is normally used to characterize an adsorbent by giving some knowledge about its surface topology as well as morphology and was used for determining the nanofiber size and shape. The morphology of the electrospun N6,6/GO nanofibers were randomly oriented in the SEM image (Fig. 5a). The elemental mapping of N6,6/GO nanofibers by EDX showed that carbon, nitrogen, and oxygen are the main elements of the nanofibers (Fig. 5b–d). The analysis displayed the existence of carbon (C), oxygen (O), and nitrogen (N) together with the wt% concentrations of 51.62, 26.18, and 22.18, respectively in EDX spectrum of N6,6/GO nanofibers (Fig. 5e).

The morphology of the electrospun Cr (VI) loaded N6,6/GO nanofibers in the SEM image (Fig. 6a) and the typical EDX spectrum of Cr (VI) loaded N6,6/GO nanofibers. The elemental mapping of N6,6/GO nanofibers by EDX showed that carbon and oxygen are the main elements of the nanocomposite. In addition, Fig. 6b–f shows the elemental mapping image regarding Cr (VI) loaded N6,6/GO nanofibers including an even distribution of C, O, N, and Cr, which further validated the successful adsorption of Cr on the surface of N6,6/GO. The elemental analysis displayed the existence of carbon (C), oxygen (O), chromium (Cr), and nitrogen (N) with the wt% concentrations 35.13, 38.69, 7.44, and 18.73 respectively (Fig. 6g).

Adsorption of Cr (VI) experiments

The Cr (VI)-adsorbent interaction was carried out as follows: the adsorption kinetics at a certain temperature was tried by adding of N6,6/GO at a dose of 0.2 g/L to a series of 10 ppm Cr (VI) solution at an initial pH of 2. The beakers were moved to the shaker (250 rpm) for different times (5 min, 15 min, 30 min, 1 h, 2 h, 4 h, 6 h, 9 h, 12 h, 18 h, and 24 h) and were maintained at 25 °C.
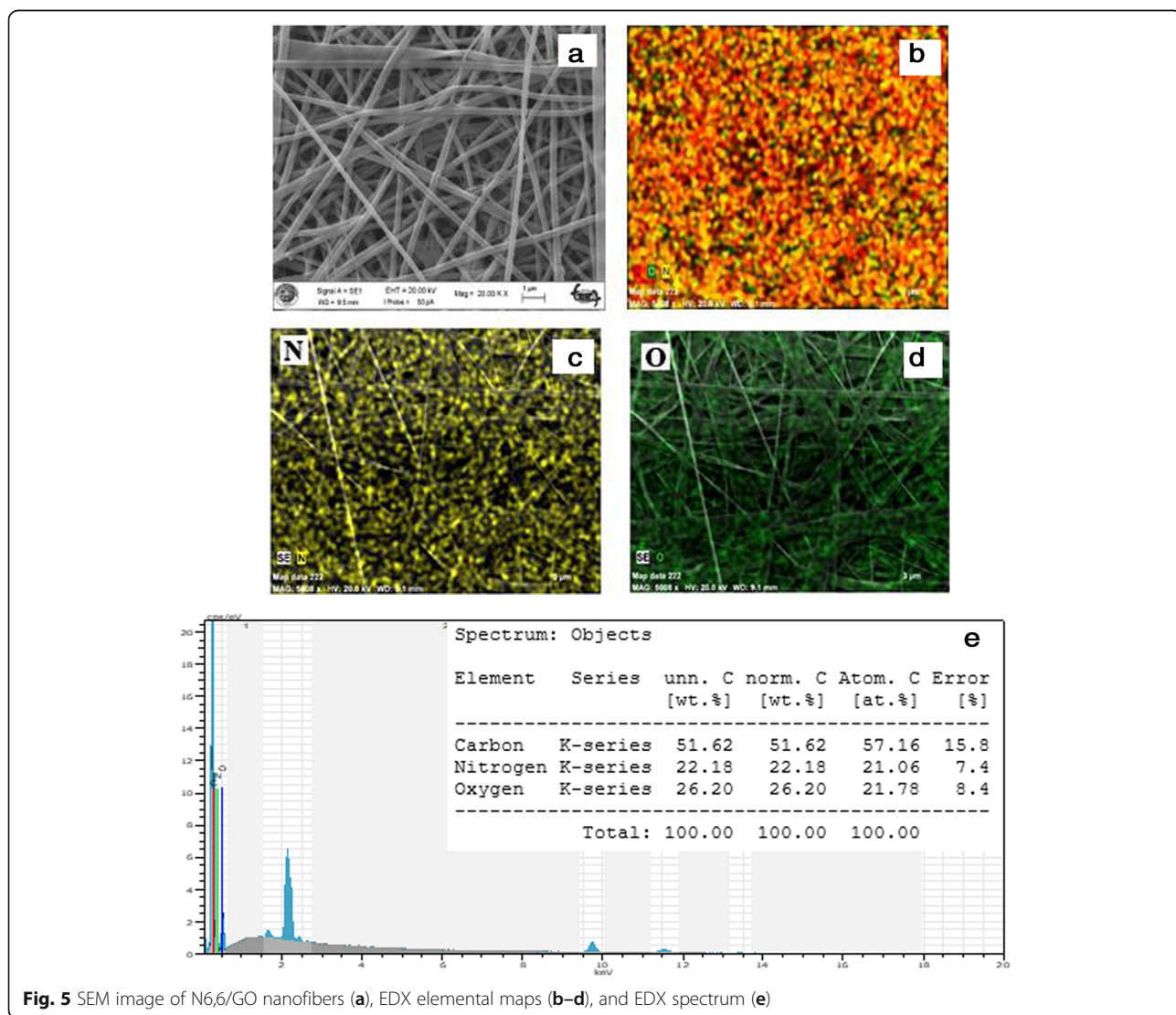

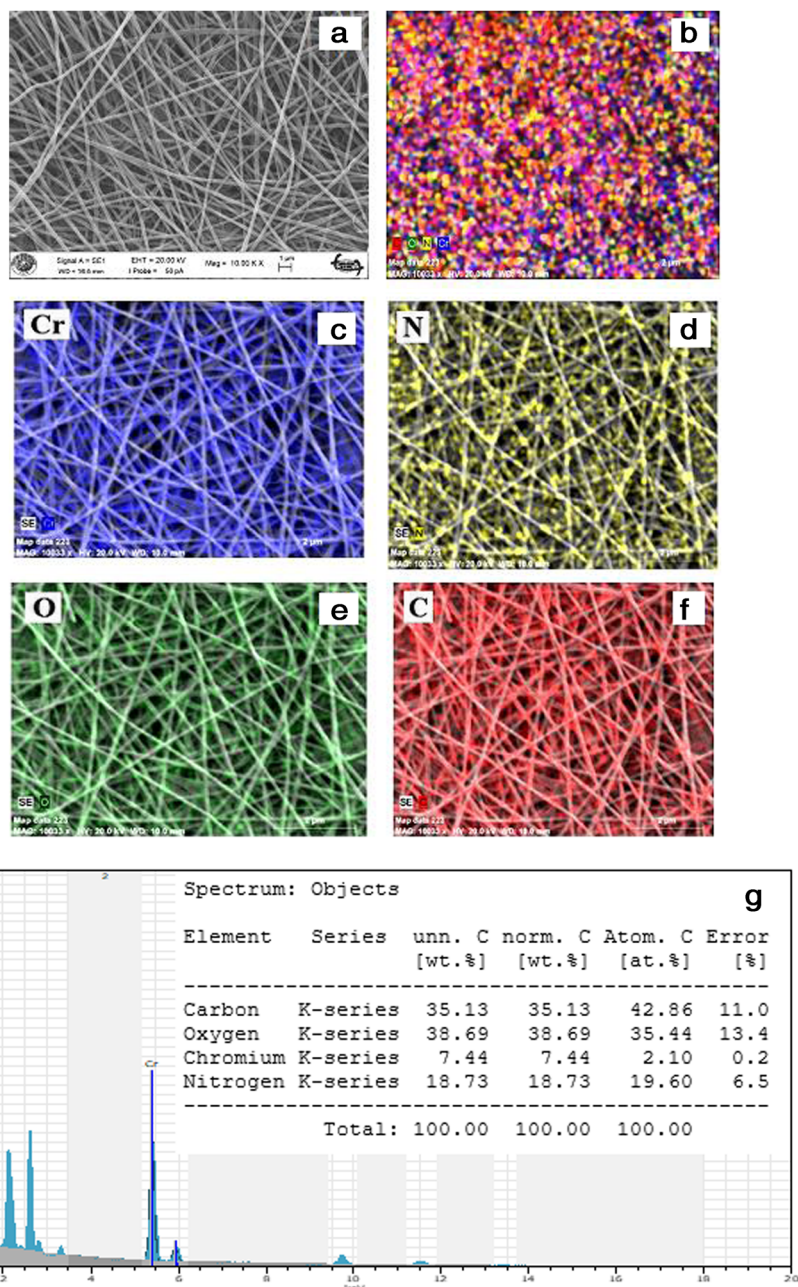**Fig. 5** SEM image of N6,6/GO nanofibers (**a**), EDX elemental maps (**b–d**), and EDX spectrum (**e**)

Fig. 6 SEM image of N6,6/GO nanofibers after Cr (VI) adsorption (**a**), EDX elemental maps (**b–f**), and EDX spectrum (**g**)

The effect of different adsorbent dose on the adsorption of Cr (VI) from the solution phase was studied by shaking 10 ppm Cr (VI) solution with the N6,6/GO (Fig. 7).

N6,6/GO dosages in the solution phase were 0.05, 0.1, 0.2, 0.3, and 0.4 g/L. The different initial concentrations of Cr (VI) (2.5, 5, 7.5, 10, 12.5, 15, and 20 ppm) were studied and initial pH of the solution was adjusted to 2. The effect of initial pH on the adsorption was studied by adding 0.2 g/L N6,6/GO to a series of beakers containing 10 ppm Cr (VI) solution and initial pH was adjusted by

adding 0.1 M NaOH and 0.1 M HCl solution from 2 to 6. The beakers were shaken (250 rpm) at room temperature for 5 h. After centrifugation, the residual Cr (VI) concentration in the supernatant liquid was analyzed spectrophotometrically at 540 nm using UV-visible spectrophotometer (ELICO-156) and 1,5 diphenylcarbazide (purity ≥ 98, Merck) as a complexing agent. Diphenylcarbazide reacts with Cr (VI) ions in acidic medium to form a purple Cr (III)-diphenylcarbazone complex (Altun et al. 2016). The maximum capacities of the

Fig. 7 Image of Nylon 6,6/graphene oxide nanofibers before and after Cr (VI) adsorption
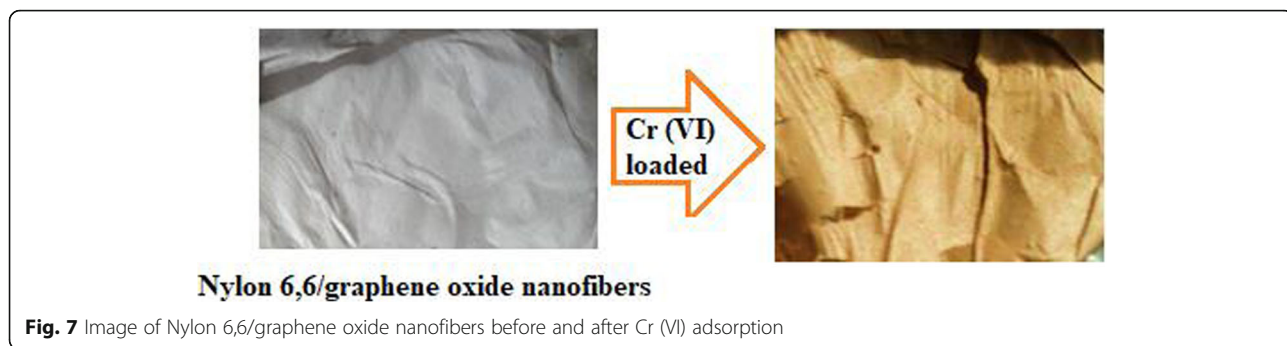
synthesized N6,6, N6,6-G, N6,6/GO (3%), N6,6/GO (5%), and Cr (VI) ions were given in Fig. 8. N6,6/G has the lowest Cr (VI) adsorption capacity. In case of using GO instead of graphene in the composite, the situation changed. That means as GO ratio increased, Cr (VI) adsorption capacity increased. For that reason, N6,6/GO (5%) was preferred as the adsorbent in the rest of the experiments.

Results and discussion

N6,6 is a widely applied thermoplastic polymer in a composite film due to its corrosion resistance, rigidity, good stability, strong insulation, high mechanical strength, and excellent load holding capacity. In addition, the low-density property makes it lighter. Nylon-6 or polycaprolactam is synthesized by ring-opening polymerization of a cyclic amide, i.e., caprolactam. It was interesting to ascertain that nylon 6,6 could be rearranged to amidoxime functions and they have good complexing properties toward metal ions in the aqueous phase (Pantchev et al. 2007).

Effect of Cr (VI) initial concentration

Figure 9 presents the adsorption isotherms at pH 2.0 as the relationship between the amount of Cr (VI) adsorbed per unit mass of a given N6,6/GO and the equilibrium concentration of Cr (VI) ions in solution. The isotherms were obtained at a starting Cr (VI) concentration range of 2.5–20 mg/L.
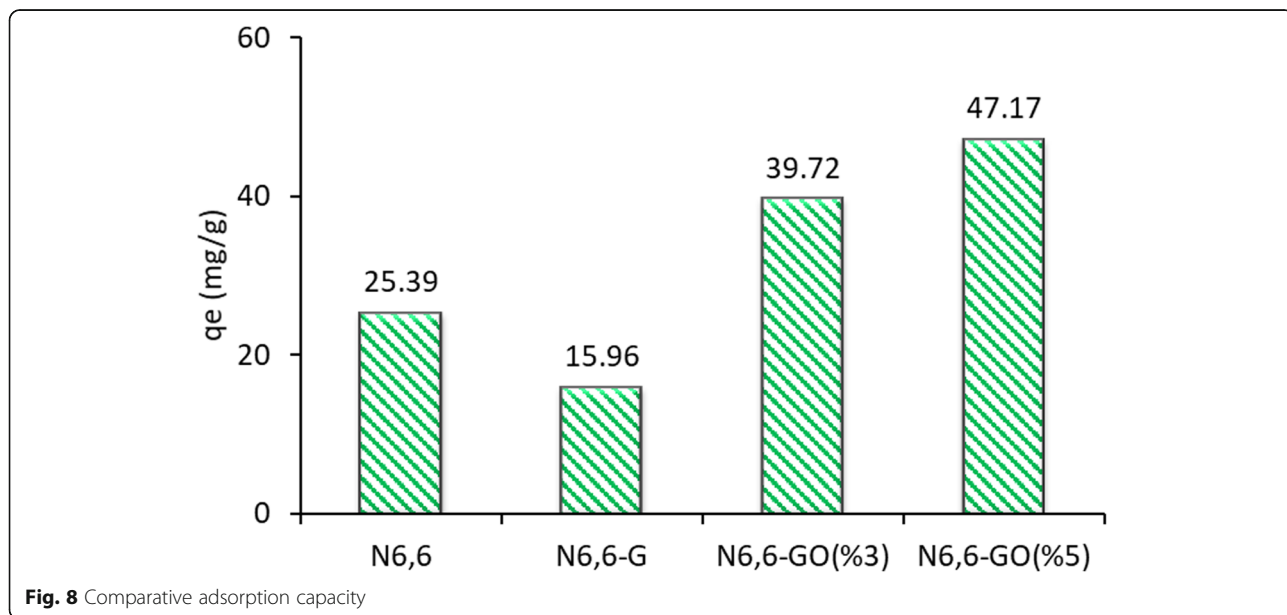
It is clear that Cr (VI) ions are better adsorbed to the N6,6/GO and the composite has an adsorption capacity of 47.17 mg/g. The Langmuir, Freundlich, Dubinin-Radushkevich, and Scatchard isotherms were used using Eqs. 1, 2, 3, and 4, respectively (Parlayıcı et al. 2015).
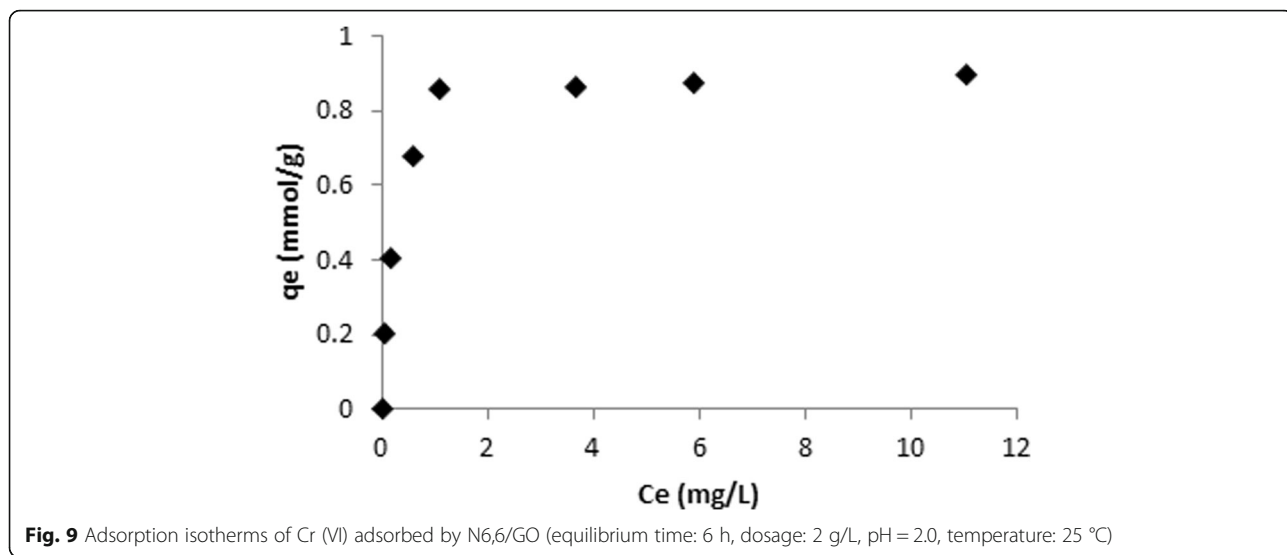
$$\frac{C_e}{q_e} = \frac{1}{K_b A_S} + \frac{C_e}{A_S} \tag{1}$$

$$\log q_e = \log K_f + \frac{1}{n} \log C_e \tag{2}$$

$$\ln q_e = \ln q_m - \beta \varepsilon^2 \tag{3}$$

$$q_e/C_e = Q_s K_s - q_e K s \tag{4}$$

Fig. 8 Comparative adsorption capacity

Fig. 9 Adsorption isotherms of Cr (VI) adsorbed by N6,6/GO (equilibrium time: 6 h, dosage: 2 g/L, pH = 2.0, temperature: 25 ℃)

q_{max} and K_L were obtained from the slope and intercept of the plot of C_e/q_e versus C_e shown in Fig. 10a. The Langmuir isotherm parameters are given in Table 1. The value of the regression R^2 obtained (0.999) showed the applicability of the isotherm.

The essential characteristics of a Langmuir isotherm can be expressed in terms of a dimensionless constant separation factor or equilibrium parameter, R_L which is defined by the following Eq. (5):

$$R_L = 1/(1 + K_L C_e) \qquad (5)$$

Where C_e is the initial concentration and R_L indicates the shape of the isotherm ($R_L > 1$ unfavorable; $R_L = 1$ linear; $0 < R_L < 1$ favorable and $R_L = 0$ irreversible). The R_L values (0.017) obtained in this study are between 0 and 1 and shows the high affinity of N6,6/GO for Cr (VI) ions. The higher determination coefficients R^2 (> 0.999) of the Langmuir equation suggest that the Langmuir equation can be
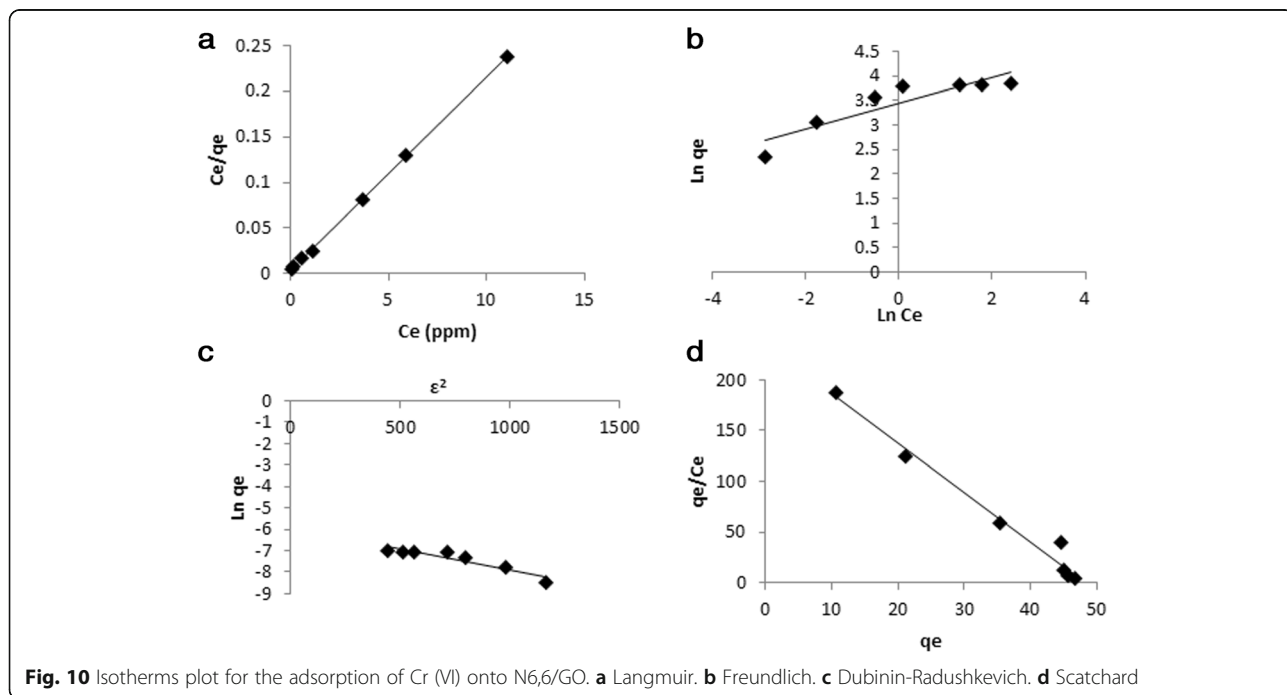

Fig. 10 Isotherms plot for the adsorption of Cr (VI) onto N6,6/GO. **a** Langmuir. **b** Freundlich. **c** Dubinin-Radushkevich. **d** Scatchard

Table 1 Equilibrium isotherm model parameters

Freundlich isotherm			Langmuir isotherm			Scatchard isotherm				D–R isotherm		
K_f	n	R^2	q_m	b	R^2	Q_s	K_s	R^2	X_m	K	E	R^2
31.41	3.79	0.814	47.17	5.73	0.999	48.49	4.82	0.978	0.003	0.002	15.81	0.863

used to fit the experimental adsorption data and to evaluate the maximum Cr (VI) ions adsorption capacity of the N6,6/GO. The results also show that the adsorption of Cr (VI) with N6,6/GO took place in a single-layer adsorption form. The linear form of the Freundlich isotherm equation is given in Eq. (2). The linear plot of lnq_e against lnC_e is shown in Fig. 10b and the constant n and K_f are calculated from the slope and intercept. The Freundlich isotherm constants are presented in Table 1. The low detection coefficients of Freundlich R^2 (0.814) indicate that isotherm data do not fit the Freundlich model.

The D-R isotherm was applied with a linear plot of lnq_e against ε^2 shown in Fig. 10c. D-R isotherm parameters are given in Table 1. When the E value is lower than 8 kJ/mol, the sorption process is said to be predominant by physical adsorption. If E is between 8 and 16 kJ/mol, the process is dominated by a chemical ion exchange mechanism and by a chemical particle diffusion (Bering et al. 1972). The E value obtained in our work is 15.81 kJ/mol indicating the chemical ion exchange process between N6,6/GO and Cr (VI) ions in the solution phase.

Adsorption isotherms were analyzed and fitted using Scatchard equation (Fig. 10d). They were used to estimate and compare the saturation capacities of N6,6/GO toward the Cr (VI) ions. When Scatchard plot is originated from linearity, more emphasis is placed on the analysis of the adsorption data in the context of the Freundlich model in order to produce the adsorption isotherms of the metal ion at certain concentrations in the solutions. To form adsorption isotherms of Cr (VI) on N6,6/GO, the adsorption characteristics were analyzed from Scatchard plot. The value of the R^2 regression (0.978) indicates that Langmuir model

can be applied for the adsorption process. Scatchard analysis of equilibrium binding data for Cr (VI) ions on N6,6/GO led to a linear plot showing that the Langmuir model could be applied in the adsorption of Cr (VI) ions.

Many investigations have been carried out on the removal of Cr (VI) from the aqueous solution (Table 2). N6,6/GO has a higher capacity for the elimination of Cr (VI) from the solution phase compared to other adsorbents.

Effect of pH

The pH value of the aqueous solution is an essential factor because it influences Cr (VI) adsorption process. pH changes the surface charge of an adsorbent and affects the ionization behavior of the adsorbent and Cr (VI) ions. The effect regarding the solution pH concerning Cr (VI) removal together with N6,6/GO is shown in Fig. 11. The removal efficiency of Cr (VI) with N6,6/GO appears to increase with pH decrease at pH range of 2.0–6.0. The maximum adsorption capacity was obtained at pH 2 and all adsorbents performed better capacity in acidic conditions than in neutral and alkaline conditions. There are various forms of Cr (VI) ion in solution, namely chromate (CrO_4^{2-}), dichromate ($Cr_2O_7^{2-}$), and hydrogen chromate ($HCrO_4^-$) (Mor et al. 2007). These ionic forms depend on the pH of the solution and on the total chromate concentration. When the pH value is less than 6.8, $HClO_4^-$ dominant species are stable and CrO_4^{2-} are stable above pH 6.8. In the acidic medium, the protonated amine exhibits big affinity for Cr (VI) in a manner of electrostatic interaction. The increase in the pH of the solution phase caused significant weakening of the electrostatic attraction between the negatively charged Cr (VI) anions by providing a negative charge of the adsorbent surface. Thus, the adsorption efficiency is reduced. Furthermore, as the pH increases, the competition between OH– and Cr (VI) ions increases.

Effect of adsorbent dosage

An optimal adsorbent dosage should be determined to maximize the interactions between Cr (VI) ions and adsorption sites of N6,6/GO in the solution phase (Konatham et al. 2013). The relationship between N6,6/GO dosage and the adsorption capacity, as much as removal efficiency of Cr (VI), are illustrated in Fig. 12. The effect of adsorbent dosage on the Cr (VI) adsorption efficiency
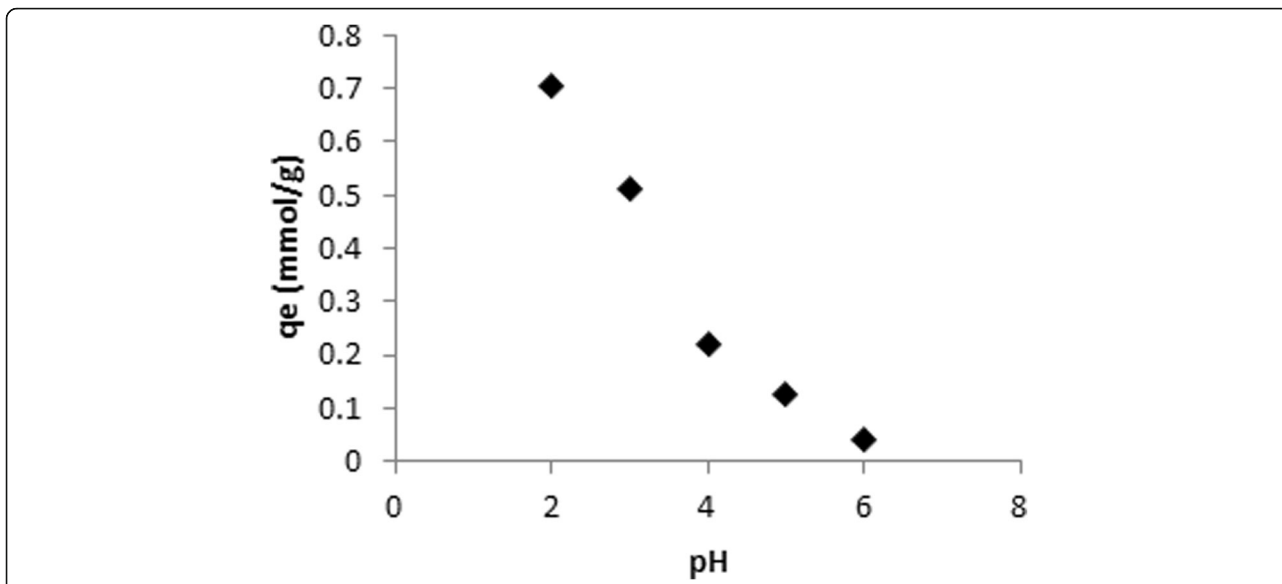
Table 2 Comparison of the adsorption capacities of Cr (VI) ions onto the various adsorbent

Adsorbent material	q_{max} (mg/g)	References
Magnetite graphene composite	5.5	Harijan and Chandra 2016
GO	13.3	Janik et al. 2018
Granular activated carbon	7	Gholipour et al. 2011
mFeOOH@AC	28.1	Su et al. 2019
Graphene modified with cetyltrimethylammonium bromide	21.57	Wu et al. 2013
N6,6/GO	47.17	This study

Fig. 11 pH effect on Cr (VI) adsorbed by N6,6/GO (equilibrium time: 6 h, dosage: 2 g/L, temperature: 25 °C)

was investigated using different amounts of adsorbent in the range of 0.05–0.4 g L^{-1}, and the results of the experiment showed that the adsorption process is strongly dependent on these parameters. The adsorption capacity of Cr (VI) follows with the increase of adsorbent dosage and a tendency has been observed in the adsorption process of N6,6/GO. Therefore, the adsorption capacity of N6,6/GO decreases from 1.16 to 0.25 mmol/g by increasing the adsorbent dosage between 0.05 and 0.4 g L^{-1}.

A relatively slow increase in the adsorbent dosage range of 0.05–0.3 g L^{-1}, Cr (VI) removal (R, %) from 44.32 to 89.21% was achieved. Figure 12 shows that the removal rate of Cr (VI) on N6,6/GO increased

remarkably with the increase of N6,6/GO dosage from 0.05 to 2.0 g L^{-1}, reaching nearly 90% at 0.2 g L^{-1}. On the other hand, the adsorption capacity of Cr (VI) on N6,6/GO was considerably reduced from 1.16 to 0.7 mmol g^{-1} as the dosage increased from 0.05 to 0.2 g L^{-1}. A further increase in the adsorbent dosage does not affect the values of the adsorption parameters. These results can be attributed to an increased adsorption dosage by providing more surface contact area and existing active adsorption sites, resulting in a higher removal percentage. A high dosage can cause agglomeration of the adsorbents (Zhang et al. 2011) and this situation was particularly true at a dosage of 0.2 g L^{-1}.
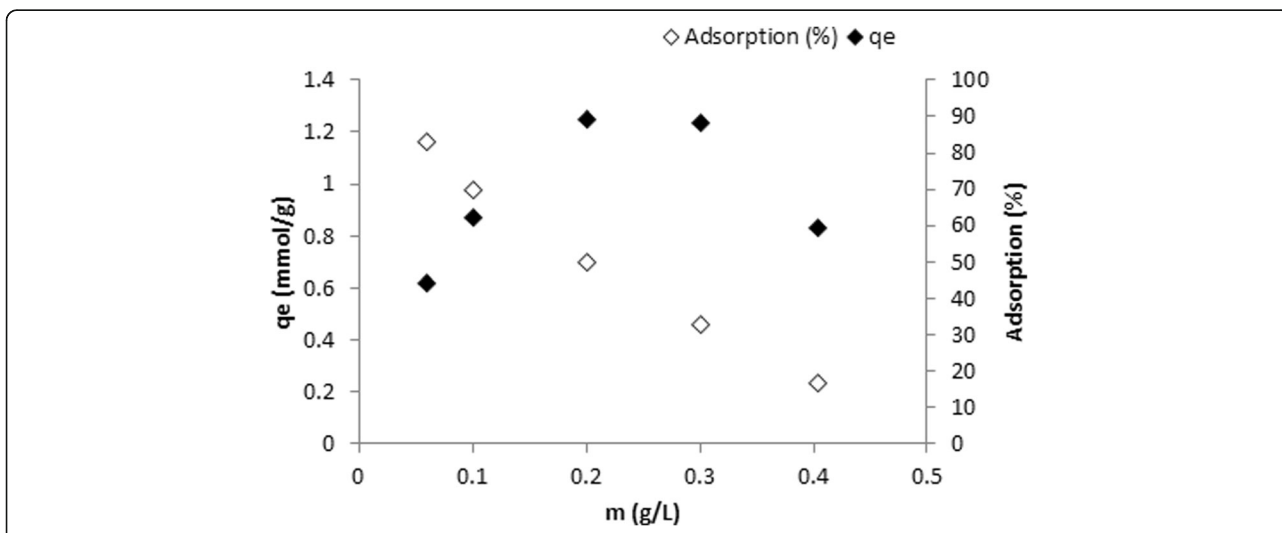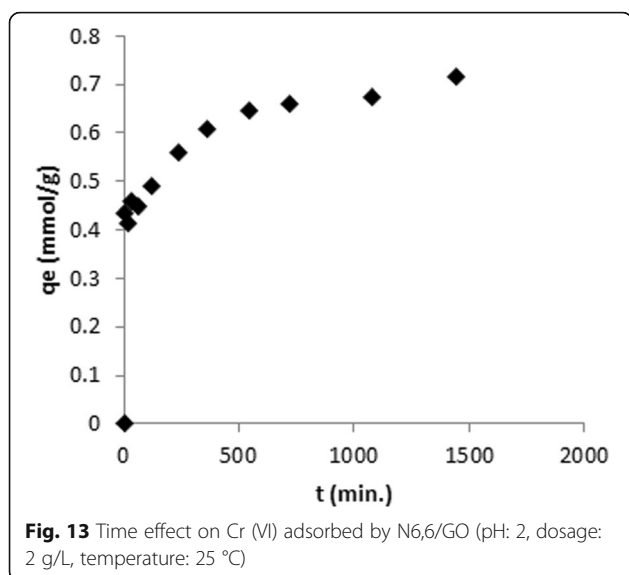

Fig. 12 Adsorbent dosage effect on Cr (VI) adsorbed by N6,6/GO (equilibrium time: 6 h, pH: 2, temperature: 25 °C)

Fig. 13 Time effect on Cr (VI) adsorbed by N6,6/GO (pH: 2, dosage: 2 g/L, temperature: 25 °C)

Effect of contact time

Figure 13 shows the effect of contact time on the uptake of Cr (VI) by N6,6/GO. In the first 60 min, Cr (VI) was taken from the solution phase quickly. The amount of Cr (VI) adsorbed on N6,6/GO grows linearly with the increase of contact time, as it can depend on many free spaces in the surface of the adsorbent. After 60 min, the Cr (VI) adsorption increased more slowly and reached equilibrium within 240 min. Cr (VI) adsorption did not change significantly with further increase in contact time. This can be a consequence of the reduction in the available active regions of the adsorbent and the

decrease in driving force (Wu et al. 2013). Based on the above results, the optimal equilibrium contact time for the following experimentation was selected as 360 min.

Adsorption kinetics

The pseudo-first-order and pseudo-second-order reaction equations were applied for the equilibrium system (Fig. 14). Pseudo-first-order kinetic model and pseudo-second-order kinetic model for Cr (VI) on N6,6/GO have been demonstrated in Table 3. The pseudo-second-order kinetic model was used based on the following differential equation: where k_2 is the rate constant of pseudo-second-order adsorption (g mg^{-1} min^{-1}). The boundary condition $q_t = 0$ at $t = 0$ and the equation can be linearized as Eq. (6):

$$\frac{1}{q_t} = \frac{1}{k_2 \, q_e 2} + \frac{1}{q_e t} \tag{6}$$

The pseudo-second-order kinetic model was found to agree between the experimental and calculated data, as indicated by the correlation coefficients higher than 0.99 obtained using this model.

Conclusions

N6,6/GO nanofibers were successfully fabricated through the electrospun method. GO was produced from graphene nanoparticle via conventional Hummers method. FT-IR and SEM-EDX were carried out to prove the successful oxidation of graphene nanoparticle into GO. Characterization of N6,6/GO nanofibers by FT-IR
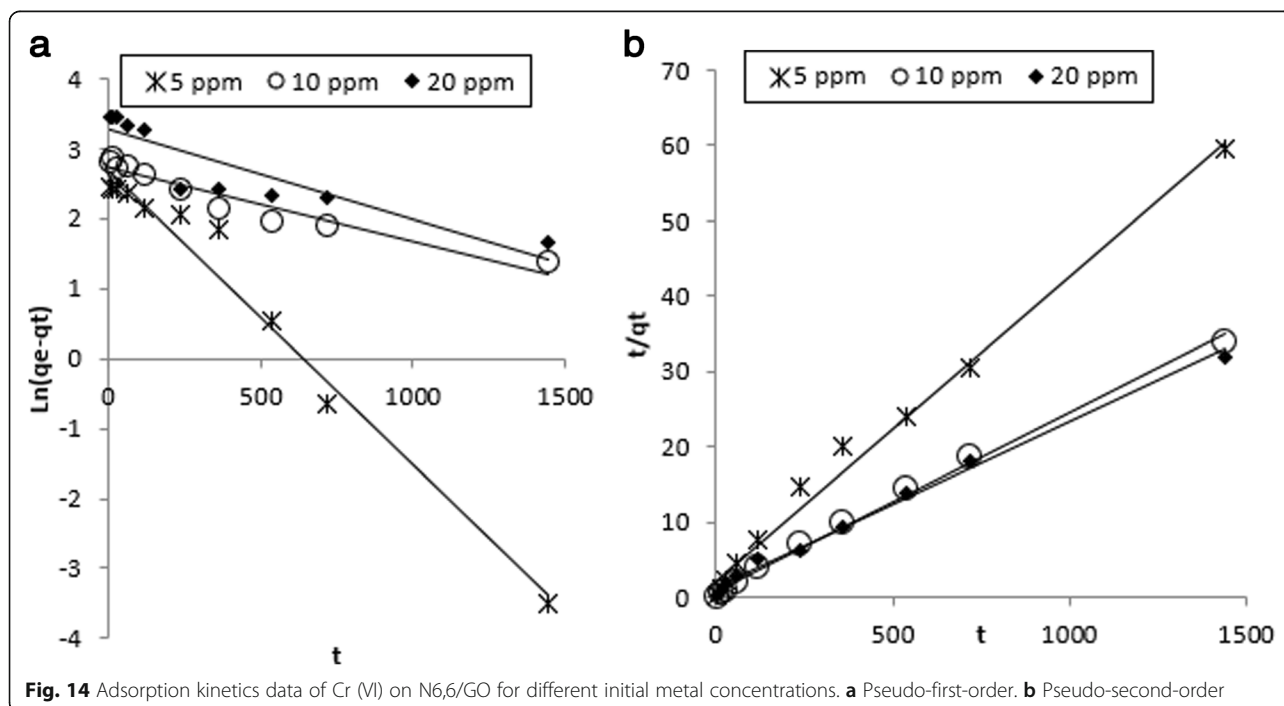

Fig. 14 Adsorption kinetics data of Cr (VI) on N6,6/GO for different initial metal concentrations. a Pseudo-first-order. b Pseudo-second-order

Table 3 Kinetic parameters of Cr (VI) adsorption N6,6/GO

C_o	q_e exp	Pseudo-first-order			Pseudo-second-order		
		k_1	q_e	R^2	k_2	q_e	R^2
5	24.18	0.0042	14.86	0.976	0.00075	24.69	0.991
10	44.31	0.0011	15.39	0.925	0.00064	42.19	0.996
20	49.31	0.0013	26.19	0.812	0.00036	45.66	0.993

indicated the presence of GO in N6,6. The adsorption behavior of Cr (VI) onto N6,6/GO nanofibers was investigated and the adsorption was found to be dependent on pH, adsorbent dosage, initial Cr (VI) concentration, and contact time. The maximum adsorption for Cr (VI) was at pH 2.0. The equilibrium between Cr (VI) and nanofibers was reached in 360 min. The equilibrium adsorption data were correlated by four adsorption isotherm equations. Isotherm analysis demonstrated that the adsorption pattern of Cr (VI) onto nanocomposite followed the Langmuir model as well as Dubinin–Radushkevich (D–R) isotherm model. Using the Langmuir model equation, the maximum capacity of N6,6/GO was identified as 47.17 mg/g.

Abbreviations
GO: Graphene oxide; N6,6: Nylon-6,6; N6,6/GO: Nylon-6,6/graphene oxide nanofibers

Availability of data and materials
Research data have been provided in the manuscript.

Authors' contributions
EP and AA conceived of the study and contributed in design and organization of the manuscript. AA produced GO and nylon-6,6/graphene oxide nanofibers. ŞP carried out the adsorption and kinetic experiments. ŞP and EP performed the data analysis. EP and AA did the manuscript writing and execute the data interpretation. All authors read and approved the final manuscript.

Competing interests
The authors declare that they have no competing interests.

Publisher's Note
Springer Nature remains neutral with regard to jurisdictional claims in published maps and institutional affiliations.

Author details
[1]Department of Chemical Engineering, Konya Technical University, 42079 Konya, Turkey. [2]Department of Biomedical Engineering, Necmettin Erbakan University, 42079 Konya, Turkey.

References
Altun T, Parlayıcı S, Pehlivan E. Hexavalent chromium removal using agricultural waste rye husk. Desalin Water Treat. 2016;57:17748–56.
Bamgbose JT, Adewuyi S, Bamgbose O, Adetoye AA. Adsorption kinetics of cadmium and lead by chitosan. African J Biotech. 2010;9:2560–5.
Bering BP, Dubinin MN, Serpinsky VV. On thermodynamics of adsorption in micropores. J Colloid and Inter Sci. 1972;38:185–94.
Charles J, Ramkumaar GR, Azhagiri S, Gunasekaran S. FTIR and thermal studies on nylon-66 and 30% glass fibre reinforced nylon-66. J Chem. 2009;6(1):23–33.
Chen L, Li Y, Chen L, Li N, Dong C, Chen Q, Liu B, Ai Q, Si P, Feng J, Zhang L, Suhr J, Lou J, Ci L. A large-area free-standing graphene oxide multilayer membrane with high stability for nanofiltration applications. Chem Eng J. 2018;345:536–44.
Chen W, Yan L, Bangal PR. Bangal, preparation of graphene by the rapid and mild thermal reduction of graphene oxide induced by microwaves. Carbon. 2010;48:1146–52.
Coiai S, Passaglia E, Pucci A, Ruggeri G. Nanocomposites based on thermoplastic polymers and functional nanofiller for sensor applications. Materials. 2015;8: 3377–427.
Gerçel Ö, Özcan A, Özcan AS, Gercel HF. Preparation of activated carbon from a renewable bio-plant of Euphorbia rigida by H2SO4 activation and its adsorption behavior in aqueous solutions. Appl Sur Sci. 2007;253(11):4843–52.
Gholipour M, Hashemipour H, Mollashahi M. Hexavalent chromium removal from aqueous solution via adsorption on granular activated carbon: adsorption, desorption, modeling and simulation studies. J Eng Appl Sci. 2011;6:10–8.
Hafez A, El-Manharawy S. Design and performance of the two-stage/two-pass RO membrane system for chromium removal from tannery wastewater, part 3. Desalination. 2004;165:141–51.
Haggenmueller R, Du F, Fischer JE, Winey KI. Winey, interfacial in situ polymerization of single wall carbon nanotube/nylon 6,6 nanocomposites. Polymer. 2006;47:2381–8.
Harijan DK, Chandra V. Environment friendly synthesis of magnetite–graphene composite for adsorption of toxic chromium (VI) ions from drinking water. Env Prog Sus Energy. 2016;35(3):700–5.
He D, Peng Z, Gong W, Luo Y, Zhao P, Kong L. Mechanism of a green graphene oxide reduction with reusable potassium carbonate. RSC Adv. 2015;5(16): 11966–72.
Huang X, Gao N, Hang Z. Thermodynamics and kinetics of cadmium adsorption onto oxidized granular activated carbon. J Env Sci. 2007;19(11):1287–92.
Janik P, Zawisza B, Talik E, Sitko R. Selective adsorption and determination of hexavalent chromium ions using graphene oxide modified with amino silanes. Micro Acta. 2018;185(2):117.
Konatham D, Yu J, Ho TA, Striolo A. Simulation insights for graphene-based water desalination membranes. Langmuir. 2013;29:11884–97.
Korus I, Loska K. Removal of Cr(III) and Cr(VI)ions from aqueous solutions by means of polyelectrolyte enhanced ultrafiltration. Desalination. 2009;247:390–5.
Liu H, Xie S, Liao J, Yan T, Liu Y, Tang X. Novel graphene oxide/bentonite composite for uranium (VI) adsorption from aqueous solution. J Radioanal Nucl Chem. 2018;317(3):1349–60.
Luo JJ, Lü QF. Controllable preparation and heavy-metal-ion adsorption of lignosulfonate-polypyrrole composite nanosorbent. Polym Compos. 2015; 36(8):1546–56.
Ma YX, Li YF, Yang LQ, Zhao GH. Preparation and characterization of polysulfone/ graphite nanosheets composites capsules for the adsorption of phenol in aqueous solution. Polym Compos. 2013;34(2):204–13.
Menchaca C, Manoun B, Martínez-Barrera G, Castaño VM, López-Valdivia H. In situ high-temperature Raman study of crystalline nylon 6,12 fibers gamma-irradiated in argon atmosphere. J Phy Chem Sol. 2006;67(9–10):2111–8.
Mor S, Ravindra K, Bishnoi NR. Adsorption of chromium from aqueous solution by activated alumina and activated charcoal. Bioresour Technol. 2007;98:954–7.
Nataraj SK, Hosaman KM, Aminabhavi TM. Potential application of an electrodialysis pilot plant containing ion-exchange membranes in chromium removal. Desalination. 2007;217:181–90.
Nirmala R, Navamathavan R, Kim HY, Park SJ. Electrical properties of conductive nylon66/graphene oxide composite nanofibers. J Nanosci Nanotech. 2015; 15(8):5718–22.
Oehmen A, Vergel D, Fradinho J, Reis MA, Crespo JG, Velizarov S. Mercury removal from water streams through the ion exchange membrane bioreactor concept. J Hazar Mater. 2014;264:65–70.
Pantchev I, Farquet P, Surbeck H, Meyer T. Surface modified nylon 6,6 and application for adsorption and detection of uranium in potable water. React Func Poly. 2007;67(2):127–35.
Panuccio MR, Sorgonà A, Rizzo M, Cacco G. Cadmium adsorption on vermiculite, zeolite and pumice: batch experimental studies. J Env Manag. 2009;90(1): 364–74.

Parlayıcı S, Eskizeybek V, Avcı A, Pehlivan E. Removal of chromium (VI) using activated carbon-supported-functionalized carbon nanotubes. J Nano Chem. 2015;5:255–63.

Pontiéa M, Derauwa JS, Plantiera S. Edouarda , Baillya, L. seawater desalination: nanofiltration—a substitute for reverse osmosis? Des Water Treat. 2013;51: 485–94.

Pouriayevali AS, Guo YB, VPW S. A constitutive description of the rate-sensitive response of semi-crystalline polymers. Inter J Impact Eng. 2013;62:35–47.

Shin EW, Karthikeyan G, Tshabalala MA. Adsorption mechanism of cadmium on juniper bark and wood. Bioresour Technol. 2007;98:588–94.

Shin MY, Hohman MM, Brenner M, Ruteldge GC. Experimental characterization of electrospinning: the electrical forced jet and instabilities. Polymer. 2001;42: 9955–67.

Su M, Fang Y, Li B, Yin W, Gu J, Liang H, Li P, Wu J. Enhanced hexavalent chromium removal by activated carbon modified with micro-sized goethite using a facile impregnation method. Sci Total Env. 2019;647:47–56.

Syrwade SP, Smirnov SN, Valssiouk IV, Unocic RR, Veith GM, Dai S, Mahurin SM. Water desalination using nanoporous single-layer graphene. Nature nanotech. 2015;10(5):459–64.

Vasudevan S, Lakshmi J, Sozhan G. Studies on the Al-Zn-in alloy as anode material for the removal of chromium from drinking water in electrolcoagulation process. Desalination. 2012;275:260–8.

Wu Y, Luo HJ, Wang H, Wang C, Zhang J, Zhang ZL. Adsorption of hexavalent chromium from aqueous solutions by graphene modified with cetyltrimethylammonium bromide. J Colloid Inter Sci. 2013;394:183–91.

Zhang NN, Qiu HX, Si YM, Wang W, Gao JP. Fabrication of highly porous biodegradable monoliths strengthened by graphene oxide and their adsorption of metal ions. Carbon. 2011;49:827–37.